# Thin film heterostructures based on Co/Ni synthetic antiferromagnets on polymer tapes: towards a sustainable flexible spintronics

**Mariam Hassan[1,2], Sara Laureti[1*], Christian Rinaldi[3], Federico Fagiani[3], Gianni Barucca[4], Francesca Casoli[5], Alessio Mezzi[6], Eleonora Bolli[6], S. Kaciulis[6], Mario Fix[2], Aladin Ullrich[2], Manfred Albrecht[2], Gaspare Varvaro[1*]**

[1]ISM - CNR, nM[2]-Lab, Area della Ricerca Roma 1, Monterotondo Scalo (Roma), 00015, Italy
[2]Institute of Physics, University of Augsburg, Universitätsstraße 1 Nord, D-86159 Augsburg, Germany
[3]Department of Physics, Politecnico di Milano, via G. Colombo 81, 20133 Milano, Italy
[4]Department SIMAU, University Politecnica delle Marche, Via Brecce Bianche, Ancona 60131, Italy & UdR INSTM Ancona
[5]IMEM - CNR, Parco Area delle Scienze 37/A, Parma 43124, Italy
[6]ISMN - CNR, Area della Ricerca Roma 1, Monterotondo Scalo (Roma), 00015, Italy

*Corresponding authors: gaspare.varvaro@ism.cnr.it, sara.laureti@ism.cnr.it

## Abstract

Synthetic antiferromagnets with perpendicular magnetic anisotropy (PMA-SAFs) have gained a growing attention for both conventional and advanced spin-based applications. While the progress of PMA-SAF spintronic devices on rigid substrates has been remarkable, only few examples on flexible thin film heterostructures are reported in the literature, all containing platinum group metals (PGMs). Systems based on Co/Ni may offer additional advantages with respect to devices containing PGMs, e.g., low damping and high spin polarization. Moreover, limiting the use of PGMs may relieve the demand for critical raw materials and reduce the environmental impact of related technologies, thus contributing to the transition towards a more sustainable future. Here we discuss the realization of Co/Ni-based PMA-SAFs and exploit it to obtain perpendicularly magnetized spin-valves (SVs) with giant magnetoresistance on flexible polyethylene naphthalate tapes. Several combinations of buffer and capping layers (i.e., Pt, Pd and Cu/Ta) are also investigated. High quality flexible SAFs with a fully compensated antiferromagnetic region and SVs with a sizeable GMR ratio, in line with the values reported in the literature for similar systems on rigid substrates, have been obtained in all cases. However, we demonstrate that PGMs allow achieving the best results when used as buffer layer, while Cu is the best choice as capping layer to optimize the properties of the stacks. We justify the role of buffer and capping layers in terms of different interdiffusion mechanisms occurring at the interface between the metallic layers. These results, along with the high robustness of the samples' properties against bending (up to 180 °), indicate that complex and bendable Co/Ni-based heterostructures with reduced content of PGMs can be obtained on flexible tapes, allowing for the development of novel flexible and sustainable spintronic devices for applications in many fields including wearable electronics, soft robotics, and biomedicine.

Keywords: Flexible spintronics, Co/Ni, Synthetic antiferromagnets, GMR, diffusion, STEM

## 1. Introduction

Antiferromagnetic (AF) materials have acquired increasing relevance over the past years as passive elements in spintronic devices for data storage/processing technologies and sensors[1,2]. To expand the range of applications of antiferromagnets, great efforts have been recently dedicated to the manipulation of AF spins with the aim to develop ferromagnetic-free functional devices based on AF materials as active spin-dependent elements[3–5]. As compared to conventional ferromagnetic spintronics, AF spintronic devices have several advantages including a high robustness against external magnetic perturbation, the absence of parasitic stray fields and ultrafast operation speeds (THz regime). However, the characteristic insensitivity of AF materials to magnetic perturbations also limits the control of the magnetic order by using external magnetic fields easily accessible in a laboratory. To overcome this limitation, several strategies have been proposed, such as the use of spin polarized currents, the coupling with ferromagnetic layers and the electric field control through magnetoelectric coupling. Despite the promising results of the different approaches, there are still open questions related to the energy efficiency and heat generation as well as limitations concerning the operating speed and temperature, which currently hinder the use of antiferromagnetic spintronic devices for practical applications.

As an alternative to crystal antiferromagnets, synthetic antiferromagnets (SAFs) consisting of two or more ferro(i)magnetic (F) layers indirectly coupled through a non-magnetic (NM) middle spacer are recently attracting increasing attention for the development of novel and more efficient spintronic devices[6–10] being also of interest for biomedicine[11,12] and potentially for other applications in place of the more common used magnetic particles[13–17]. The interlayer exchange coupling (IEC) between the F layers in metallic SAFs is essentially a spin-dependent *Ruderman-Kittel-Kasuya-Yosida* (RKKY) coupling with an oscillatory behavior inducing an F and AF coupling depending on the NM layer thickness[18,19]. Its strength is typically two or more orders of magnitude smaller than the ordinary exchange coupling in crystal antiferromagnets, thus allowing for a relatively easier manipulation and control of the magnetic configuration (parallel/antiparallel alignment), while maintaining a relatively large stability. They also allow for additional tunability, as the overall magnetic properties of the SAFs can be finely tuned by changing the single layers features (e.g., materials, composition, thicknesses, etc.)[18,19], thus enabling for extra degrees of freedom for the optimization of the material performance. So far, most of the work on SAFs for spintronic applications has been focused on their use as reference electrode in giant magnetoresistance spin valves (GMR-SVs) and magnetic tunnel junctions (MTJs) as the flux-closure structure of the SAF allows reducing the undesired stray fields acting on the free-layer typically observed when AF/F reference electrodes are used[20,21]. Besides these traditional spintronic applications, SAFs have been demonstrated to be of great relevance for the development of novel spintronic devices exploiting the movement of domain walls[22] or the displacement and the size change of skyrmions [9,23–27]. Moreover, the relatively week IEC between the F layers allows the magnetic configuration to be controlled by using external electric fields[10,28,29], thus paving the way for the development of voltage-controlled spintronic devices characterized by a much lower power consumption with respect to the most investigated spintronic systems driven by electrical currents. While the first generation of SAFs relied on thin films with in-plane magnetic anisotropy, large efforts have been done to develop SAFs and related spintronic devices with perpendicular magnetic anisotropy (PMA), which are featured by a large uniaxial magnetic anisotropy

allowing for additional functionality as well as improved performance for data storage/processing technologies and sensors[30–32]. To this aim, $[Co/X]_N$ multilayer thin film stacks (where X = Pd, Pt, Ir or Ni and *N* the number of repetitions) have been extensively used as building blocks[33–41] due to their large perpendicular magnetic anisotropy (PMA) arising at the interface among the layers ($10^5$ – $10^6$ J/m$^3$)[35,42,43] and the high tuneability of the overall magnetic properties through the modulation of layers' thickness and number of repetitions[44]. Moreover, differently to other materials, such as the $L1_0$-MPt(Pd) (M = Fe, Co) binary alloys, which require high deposition temperatures and suitable underlayer/substrates to obtain the correct phase and crystallographic orientation needed to develop a PMA[45–49], $[Co/X]_N$ multilayer thin film stacks can be easily obtained at room temperature and on arbitrary substrates without losing the PMA, thus keeping the easy magnetization direction perpendicular to the Co/X interface[7,8,50,51].

Although the progress and development of spintronic devices based on PMA-SAFs on rigid substrates has been remarkable, only few studies are reported in the literature on the fabrication of such systems on flexible tapes[7,8,52], despite they would allow for additional functionality, such as light-weight, flexibility, shapeability and wearability[53]. To the best of our knowledge, all the studies reported so far rely on systems based on multilayer thin film stacks containing platinum group metals (PGMs, e.g., Pt, Pd) that allow achieving a strong and robust PMA. After the seminal work of *T. Vemulkar* and *co-authors* reporting on the fabrication of FeCoB/Pt-based PMA-SAF thin films and wires on polyimide tapes[52], we recently demonstrated that more complex heterostructures, that is PMA GMR spin-valves comprising a Co/Pd-based SAF reference electrode, can be obtained either by direct deposition on flexible polyethylene tapes[7] or by exploiting an Au-mediated transfer and bonding approach[8], thus paving the way for the development of novel spintronic devices, such as flexible magneto-receptors for human-machine interfaces as reported in Ref [7].

Aiming at widening the domain of research on flexible spintronics, this work focuses on thin film heterostructures based on the Co/Ni system, which offer additional advantages with respect to multilayers comprising PGMs, including a higher spin polarization and a low intrinsic Gilbert damping factor of around 0.02 that is quite insensitive to the bilayer composition[54]. All these features, combined with a large PMA (up to 5 MJ/m$^3$), and a moderate saturation magnetization (6 – 7 MA/m), have made Co/Ni multilayers of great interest for both conventional and next generation spintronic devices, including GMR-SVs and MTJs[55,56], domain-wall and skyrmion based electronics[22,57,58], spin wave-based devices[59] as well as spin-transfer and spin-orbit torque components[60]. Besides these technical aspects, the substitution of Co/Pt(Pd) by Co/Ni based SAFs in spintronic devices was recently demonstrated to lead to a reduction of energy requirements and costs[61] due to the reduced demand of the critical and costly PGMs. Although the economic and environmental gain is low if compared with the higher energetic and environmental costs associated to the fabrication of Si wafers, which are commonly used in electronics, the additional benefits related to the low risk of supply of Ni, makes the replacement of Co/Pt(Pd) by Co/Ni based SAFs still convenient to reduce the impact of PGMs and contribute to the general effort to transition towards a more sustainable future. Despite the high potential of Co/Ni-based SAFs, to the best of our knowledge, all the efforts have been focused so far on the use of such material in spintronic devices deposited on rigid substrates, while no examples are reported on flexible tapes.

To fill this gap, Co/Ni-based PMA-SAFs and GMR-SV thin film stacks consisting of a $[Co/Ni]_N$ free layer and a fully compensated $[Co/Ni]_N/Ru/[Co/Ni]_N$ SAF reference electrode separated by a Cu spacer were prepared by direct deposition on flexible Teonex® tapes consisting of a polyethylene naphtholate (PEN) foil (thickness: 125 μm) with a flattening coating that allow for a very good surface smoothness (average roughness < 0.7 nm, accordingly to the data sheet). This feature combined with an excellent dimensional stability, low moisture pickup, good solvent resistance and high clarity, makes Teonex® a promising substrate for subsequent vacuum and other coating processes, leading to the potential use of this material as a flexible substrate for device manufacturing[62]. To fully explore the potential of the proposed approach, different combinations of buffer and capping layers were investigated, and the magnetic properties of the systems were correlated to the interdiffusion processes occurring at the bottom and top interfaces[63,64]. The use of the non-critical Cu element was explored to replace the Pt and Pd heavy metals, typically used to support the development of a strong PMA. Cu was already demonstrated to be effective in inducing a PMA in Co/Ni-based thin film stacks on rigid substrates[65] and its successful exploitation as buffer and capping layer on a flexible PGMs-free system would pave the way toward a sustainable flexible spintronics.

## 2. Experimental details

### 2.1. Samples' preparation

Co/Ni-based SAF and GMR-SV thin film stacks (**Figure 1**) were deposited at room temperature by DC magnetron sputtering (BESTEC UHV system) on flexible Teonex® tapes (thickness: 125 μm, average roughness < 0.7 nm) supplied by *Teijin* corporation and simultaneously on thermally-oxidized Si(100) wafers (reference samples).

The first set of samples consists of SAF multilayers with the sequence $[Co(0.2)/Ni(0.7)]_6/Co(0.2)/Ru(0.4)/Co(0.2)/[Ni(0.7)/Co(0.2)]_6$ (thicknesses in nanometres), deposited by using different combinations of buffer and capping layers (Pd, Pt, Cu) as summarized in **Table 1**. The Ru thickness was set to 0.4 nm to maximize the antiferromagnetic coupling[7,8,12], while the Co and Ni layer thickness and the bilayer repetition number *N* were fixed for all samples at 0.2 nm, 0.7 nm and 6, respectively, to ensure a high PMA, a wide AF coupled region and a low damping in the system[35,36,65]. Furthermore, GMR-SVs consisting of a $[Co(0.2)/Ni(0.7)]_6/Co(0.2)/Ru(0.4)/Co(0.2)/[Ni(0.7)/Co(0.2)]$ SAF reference layer (SAF-RL) and a $[Co(0.2)[Ni(0.7)]_{N_{FL}}/Co(0.2)$ free-layer (FL) separated by a 3-nm thick Cu spacer were prepared by using different buffer and capping layers (**Table 1**). The bilayer repetition number in the free layer ($N_{FL}$) was set to 2 for all the samples except for those grown on Pt and covered with a Pt capping layer, for which $N_{FL}$ was varied from 2 and 4, as will be discussed in detail later.

A 10-nm thick Ta seed layer was inserted in all the samples to induce a (111) crystallographic texture, which provides a strong PMA in the in the multilayer system[65,66]. In addition, samples with a Cu capping layer were also covered with a 3-nm thick Ta protecting layer to limit the Cu oxidation. The deposition rates of each material were set to 0.025 $nm \cdot s^{-1}$ (52 W-DC) for Co, 0.02 $nm \cdot s^{-1}$ (35 W-DC) for Ni, 0.03 $nm \cdot s^{-1}$ (40 W-DC) for Ta, 0.05 $nm \cdot s^{-1}$ (37 W-DC) for Pt, 0.04 $nm \cdot s^{-1}$ (26 W-DC) for Pd, 0.04 $nm \cdot s^{-1}$ (29 W-DC) for Cu and 0.025 $nm \cdot s^{-1}$ (49 W-DC) for Ru.

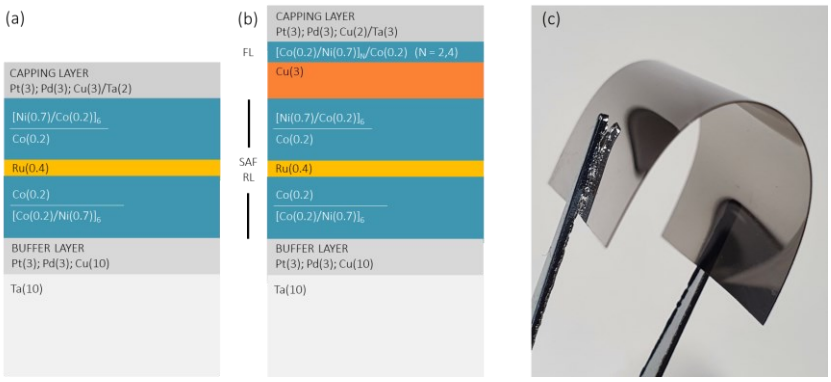


**Figure 1**. Sketch of Co/Ni-based (a) synthetic antiferromagnets and (b) GMR spin valve stacks consisting of a synthetic antiferromagnet reference electrode (SAF-RL) and a free-layer (FL) separated by a Cu spacer; thicknesses are in nanometres. (c) Photograph of a flexible Co/Ni-based thin film stack.

**Table 1**. Summary of the investigated thin film samples. The buffer and capping layers sandwiching the magnetic stacks are indicated in bold. All the thicknesses are reported in nanometres.

| **Buffer layer / Magnetic Stack / Capping layer** | |
|---|---|
| SAF Structure | SAF-based GMR-SV Structure |
| **Pt**(3)/SAF/**Pt**(3) | **Pt**(3)/SAF-RL/$Cu_{spacer}$/FL/**Pt**(3) |
| **Pt**(3)/SAF/**Cu**(2)/Ta(3) | **Pt**(3)/SAF-RL/$Cu_{spacer}$/FL/**Cu**(2)/Ta(3) |
| **Pd**(3)/SAF/**Pd**(3) | **Pd**(3)/SAF-RL/$Cu_{spacer}$/FL/**Pd**(3) |
| **Pd**(3)/SAF/**Cu**(2)/Ta(3) | **Pd**(3)/SAF-RL/$Cu_{spacer}$/FL/**Cu**(2)/Ta(3) |
| **Cu**(10)/SAF/**Cu**(2)/Ta(3) | **Cu**(10)/SAF-RL/$Cu_{spacer}$/FL/**Cu**(2)/Ta(3) |

## 2.2. Characterization

Room temperature field-dependent magnetization loops were measured by using both superconductive interference device – vibrating sample magnetometry (SQUID-VSM, LOT-QuantumDesign, MPMS3) and VSM (Microsense, Model 10) with the magnetic field applied along the film normal. Magnetic measurements under bending conditions were performed by mounting the samples on a customized semi-cylindrical plastic support with the proper radius of curvature.

Magneto-resistance versus magnetic field was measured on square-shaped samples by using the van der Pauw method[67], with a current-in-plane geometry and the external magnetic field perpendicular to the sample surface, i.e. along the easy axis of the magnetic structure. The injected current was always in the order of 10 mA and provided by a Keithley 6221 current source, while the corresponding voltages were measured by a Keithley 2182A nanovoltmeter. The magnetic field was applied through a standard electromagnet.

The surface chemical composition of the samples was investigated by X-ray photoelectron spectroscopy. The XPS measurements were performed by using an ESCALAB 250Xi, equipped with a monochromatized Al K⍰ (h⍰ = 1486.6 eV) source, electromagnetic lens mode and six channeltron

detection system. The measurements were carried maintaining the pressure in the main chamber at P = $10^{-8}$ mbar and it was increased up to P = $10^{-6}$ Pa, during the depth profile. The XPS depth profile was realized combining cycles of ion sputtering and spectra acquisition. The ion sputtering was performed with an $Ar^+$ ion gun EX-06, which energy was set at 0.5 keV and a med value of beam current 2µmA.The spectra were acquired at constant pass energy of 40 eV, while the zero point of the binding energy (BE) scale was calibrated by measuring the level Fermi at 0 eV for metals. All spectra were collected and processed by Avantage v.5979 software.

Transmission electron microscopy (TEM) and scanning transmission electron microscopy (STEM) analyses were performed on reference samples (Si substrates) by using a Philips CM200 microscope as well as a JEOL NEOARM 200F (equipped with a JEOL energy dispersive X-ray (EDX) detector), both operating at 200 keV beam energy. The EDS measurements were performed in the scanning mode (STEM) on the JEOL NEOARM. For data acquisition and quantification, the Digital Micrograph Software (GATAN) was used. For (S)TEM observations, cross-sectioned samples were prepared by the conventional thinning procedure consisting of mechanical polishing by grinding papers, diamond pastes and a dimple grinder. Final thinning was carried out by an ion beam system (Gatan PIPS) using Ar ions at 5 kV.

## 3. Results

### 3.1. Magnetic properties of flexible Co/Ni-based SAFs

The out-of-plane field-dependent magnetization loops of Co/Ni-based SAF thin film stacks deposited on flexible Teonex® tapes with different buffer and capping layers are reported in **Figures 2**. In all the samples, two distinct minor loops of the same amplitude are present, corresponding to the individual switching of the magnetization of the top and bottom Co/Ni ferromagnetic layers. They are separated by a wide antiferromagnetic-coupled field region with a (almost) zero moment in the whole field range, thus indicating that (almost) fully compensated antiferromagnetic thin film stacks were obtained. Despite the samples show similar loop shapes, some key differences can be observed. When the same metal is used as both the buffer and capping layer (**Figures 2a**, **2b** and **2c**), the interlayer exchange coupling field $H_{ex}$, defined as the field shift of the minor loop (see inset of **Figure 2a**), is larger for the Pt/SAF/Pt thin film stack and reaches the lowest value in the Pd/SAF/Pd sample (**Figure 2f** and **Table S1** in the *Supporting Information*). In the latter case, the field dependent magnetization loop also presents a superimposed positive slope, which suggests a partial tilting of the magnetic easy axis. When the non-critical Cu metal is used, an intermediate $H_{ex}$ is observed along with a non-perfect compensation of the synthetic antiferromagnet, which may be ascribed to a small difference in the magnetic thickness of the two layers, with the one with the larger value switching first. Replacing the capping layer of Pt and Pd by Cu (**Figures 2d** and **2e**, respectively) a similar trend is observed, i.e., the structure with Pt as buffer layer features the highest value of $H_{ex}$. Moreover, the Cu capping layer results beneficial in enhancing both loop squareness and interlayer exchange field, thus suggesting it contributes to stabilizing the perpendicular magnetic anisotropy of the Co/Ni multilayer. The reason of the observed differences may be ascribed to changes in the growth

morphology between the three metals, which is reflected in different features of the buffer/SAF interface, as discussed later in the text.

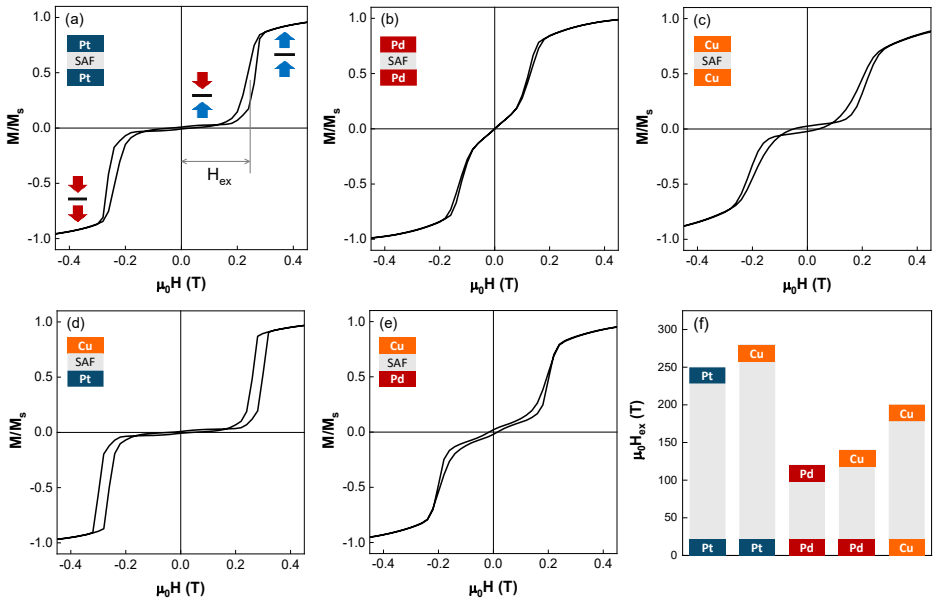


**Figure 2**. (a – e) Out-of-plane field-dependent magnetization loops of Co/Ni-based SAF thin film stacks deposited on flexible Teonex® tapes with different buffer and capping layers: (a) Pt/SAF/Pt, (b) Pd/SAF/Pd, (c) Cu/SAF/Cu, (d) Pt/SAF/Cu, (e) Pd/SAF/Cu. All measurements were performed at room temperature and normalized to the saturation magnetization ($M_s$). The arrows reported in (a) denote the mutual alignment of the magnetization in the bottom and top layer of the SAF at different points in the loop; the same evolution of the magnetic configuration is observed in all the samples. (f) Interlayer exchange field $H_{ex}$ (defined as the field shift of the minor loop, inset of Figure a) for different combinations of buffer and capping layers.

Despite the larger surface roughness of Teonex® tapes (~0.7 nm) with respect to that of commonly used SiOx/Si(100) rigid substrates (0.2 – 0.3 nm)[7], flexible SAFs present very similar behaviour of the reference samples deposited on $SiO_x$/Si(100) (**Figure S1**, *Supporting Information*) except for a less sharp magnetization switching of the top and bottom Co/Ni ferromagnetic layers and slightly lower $H_{ex}$ values (**Table S1,** *Supporting Information*). These small differences are likely due to the larger surface roughness and the presence of surface defects of Teonex® tapes[62].

To explore the possibility to integrate such flexible systems on curved surfaces, magnetic measurements were performed by folding the samples both inward and outward under a bending angle $\vartheta$ = 180° and at a curvature $\kappa = 1/r = 0.4$ mm$^{-1}$ ($r$: bending radius) that is in line with the values commonly reported in the literature for the characterization of flexible spintronic materials[29]. As a representative case, the field-dependent magnetization loops under bending of Pt/SAF/Cu flexible SAFs showing the best properties are reported in **Figures 3a** and **3c**, along with that of the flat thin

film stack (**Figures 3b**). The characteristic two-steps behaviour of perpendicular magnetized SAFs and a fully compensated AF-coupled region are retained. However, the bending leads to slanted loops accompanied by slight changes of the interlayer exchange coupling field, minor loop coercivity and loop squareness. Despite these changes can be mainly attributed to the film's curvature that induces local distribution of the magnetic easy axis with respect to the external applied field[8], the small differences between the loops measured under inward and outward bending suggests that the magnetic properties are also slightly affected by the lattice distortion of the SAF, which depends on the folding configuration. Indeed, the concave bending results in a compressive strain in the film plane and a tensile deformation along the film thickness, while the opposite situation occurs when the SAF is under a convex bending. The two bending configurations result then in opposite strain effects, which may lead for example to a weakening or a straightening either of the interlayer exchange coupling (due to a change of the Ru thickness)[29] or the magnetic anisotropy (due to a modulation of the magneto-strictive contribution to the total magnetic energy)[68] with a consequent modification of the field-dependent magnetic response.

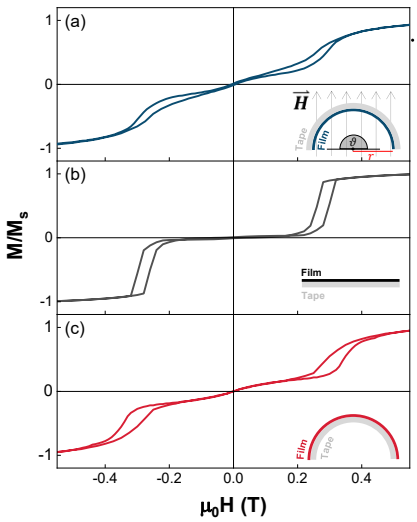


**Figure 3.** (a, c) Field-dependent magnetization loops of Pt/SAF/Cu samples measured under (a) inward and (c) outward bending ($\vartheta$ = 180°, $\kappa = 1/r$ = 0.4 mm$^{-1}$). The samples are placed in a uniform magnetic field aligned as schematized in the inset of Figure a. The out-of-plane hysteresis loop of the flat sample is also displayed in (b) as comparison. All measurements were performed at room temperature and normalized to the saturation magnetization ($M_s$).

### 3.2. Magnetic and magneto-transport properties of flexible Co/Ni-based GMR spin-valves

Pt/SAF/Cu, Pd/SAF/Cu and Cu/SAF/Cu thin film stacks are used as reference-layer/spacer (SAF-RL/$Cu_{spacer}$) of the Co/Ni-based GMR-SVs. The Cu layer, which was previously used as capping layer, is now turned into the non-magnetic spacer of the GMR spin-valve. The Cu layer is then sandwiched

between two Co layers belonging to the SAF-RL (bottom interface) and the Co/Ni-based FL (top interface). As in the previous set of samples, symmetric Pt/SAF/$Cu_{buffer}$/FL/Pt and Pd/SAF/$Cu_{buffer}$/FL/Pd samples were firstly compared to assess the effect of the two different heavy metals. The out-of-plane field-dependent magnetization loops of the two flexible spin-valves (**Figures 4a** and **4b**, top panels) show a three-steps behaviour associated to the individual reversal of the FL and the bottom and top layers of the SAF-RL. While no significant differences are present in the high-field region, a clear effect of the capping layer on the FL loop shape was observed. The Pd contributes indeed to the stabilization of the PMA, as suggested by the almost squared hysteresis loop, while, when a Pt capping layer is used, the loop becomes anhysteretic indicating the free layer lost the PMA with a consequent rotation of the magnetization from two opposite out-of-plane directions. As previously observed, the capping layer may have a considerable effect on the stabilization of the PMA of thin ferromagnetic films, mainly due to different interdiffusion mechanisms occurring during post-deposition thermal treatments[69,70]. Indeed, it has been recently demonstrated that interdiffused interfaces can develop during sputter deposition even at room temperature owing to a series of exchange events of atoms occurring during the film growth, which are strongly dependent on the chemical nature of the two materials involved in the process[64]; how this applies to the present work will be deeply discussed in the following section. The corresponding magneto-resistive curves of the two samples are presented in the bottom panels of **Figures 4a** and **4b**. The curve of the Pd/SAF/$Cu_{buffer}$/FL/Pd sample shows the typical behaviour expected for a PMA spin-valve with a SAF reference layer. The change in resistance normalized to its lowest value, $\Delta R/R_{low} = (R_{high} - R_{low})/R_{low}$, sudden increases in correspondence to the first jump in the *M*(*H*) loop thus indicating that the top SAF-RL switches first likely because of a slightly higher magnetic anisotropy of the *bottom* SAF-RL that is directly grown on the Ta seed layer[8]. The resistance then sharply reduces to its minimum value in correspondence with the magnetization reversal of the FL. A maximum GMR ratio of ~3 % is measured, which is in line with values reported in the literature for similar Co/Ni-based SVs on rigid substrates[71]. The Pt/SAF/$Cu_{buffer}$/FL/Pt sample shows a similar behaviour in the high-field region; however, in the low field region, the resistance, instead of showing a sharp reduction, as observed in the Pd-based sample, gradually reduces because of the rotation of the magnetization of the free layer during the field sweep.

Following the approach applied for the SAF samples, i.e., with the aim of reducing the use of the PGMs, Cu metal was then used to substitute Pt and Pd as capping layer and, lastly, as both the buffer and capping layers. In asymmetrical SVs with Pd and Pt buffer layers, the use of a Cu caping layer allows stabilizing the PMA of the Co/Ni free layer, as evidenced in **Figures 4d** and **4e** by the increase of free layer loop squareness for both the samples. Moreover, the substitution of high Z elements (Pd, Pt), which produce a low spin polarization, is also reflected in an increase of the GMR value (**Figure 4f**). However, in fully Cu-substituted SAF GMR-SVs, a slightly reduction of the GMR is observed, likely because of a worsening of the interface quality induced by the Cu buffer layer as will be discussed in detail later in more details.

Despite the higher surface roughness of Teonex® tapes with respect to commonly used SiOx/Si(100) rigid substrates, high-quality flexible GMR spin valves with properties very close to those of reference samples (**Figure S2** and **Table S2**, *Supporting Information*) were successfully obtained on flexible polymeric substrates regardless of the complexity of the prepared heterostructure and the presence

of very thin layers and many interfaces. The less sharp reversals of the individual layers, which in turn reflect in the shape of the corresponding magneto-resistance curves that appear rounded rather than straight, and the slightly lower but still high GMR values of flexible SVs may result from the larger surface roughness and the presence of surface defects of Teonex® tapes[62].

To explore the possibility to integrate such flexible systems on curved surfaces, magnetization measurements were performed on curved sample under the same conditions used for the SAF thin film stacks (i.e., $\vartheta$ = 180°, curvature $\kappa = 1/r = 0.4\ mm^{-1}$). All the samples retain the PMA and the typical three-step hysteresis loop in both inward and outward configurations as reported in **Figure 5** for the Pt/SV/Cu film stack showing the best properties, as a representative example. As for the case of SAF thin film stacks, the slight changes of the loop shape as well as the small differences between inward and outward measurements may be associated to the angular dispersion of the easy axis with respect to the external magnetic field, as well as to the strain effect induced by the curvature. These small variations of the magnetic behaviour with respect to the flat samples would reflect in slightly changes of the magneto-resistive properties as already observed in similar flexible samples[8].

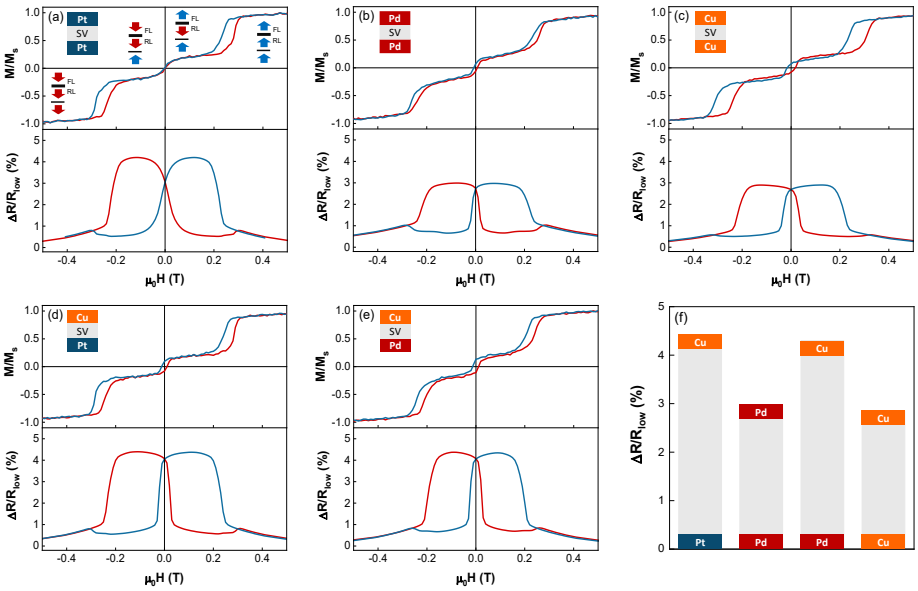


**Figure 4**. (a - e) Out-of-plane field-dependent magnetization loops (normalized to the saturation magnetization $M_s$) and corresponding magneto-resistive response ($\Delta R/R_{low}$ *vs.* $H$) of Co/Ni-based GMR-SV thin film stacks deposited on flexible Teonex® tapes with different buffer and capping layers: (a) Pt/SV/Pt, (b) Pd/SV/Pd, (c) Cu/SV/Cu, (d) Pt/SV/Cu, (e) Pd/SV/Cu. Different colors and symbols are used to evidence the two sweep directions of the external field (ascending red, descending blue). All measurements were performed at room temperature. The arrows marked in (a) denote the mutual alignment of the magnetization in the FL and top and bottom films of the SAF-RL. (f) Maximum GMR ratio for different combinations of buffer and capping layers; the value of the Pt/SV/Pt sample is not reported due to the lack of PMA of the free layer.

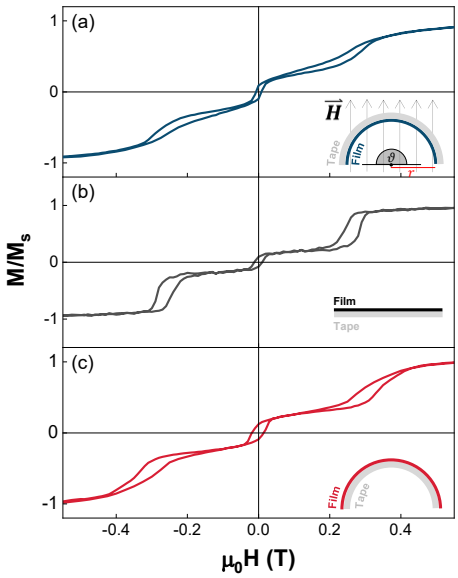


**Figure 5**. (a, c) Field-dependent magnetization loops of Pt/SV/Cu samples measured under (a) inward and (c) outward bending ($\vartheta$ = 180°, $\kappa = 1/r$ = 0.4 mm$^{-1}$). The samples are placed in a uniform magnetic field aligned as schematized in the inset of Figure a. The out-of-plane hysteresis loop of the flat sample is also displayed in (b) as comparison. All measurements were performed at room temperature and normalized to the saturation magnetization ($M_s$).

### 3.3. Chemical and microstructural properties

The analysis of magnetic and magneto-transport properties indicate that the sample's features are strongly affected by the combination of buffer and capping layers. The best performance in terms of PMA, loop coercivity and squareness and GMR ratio are obtained when samples are deposited on a Pt buffer layer and covered by a Cu capping layer. To understand the reason for this behaviour, a detailed characterization of the chemical and microstructural properties was needed.

To this purpose, X-ray photoelectron spectroscopy (XPS) was performed to investigate the surface chemical properties and the atomic concentration depth profile of the top layers in three SV thin film stacks with different capping layers (i.e., Pt/SV/Cu/Ta, Pd/SV/Pd and Pt/SV/Pt). The results reported in **Figure 6** indicate that the capping layer acts as a good protection avoiding the oxidation of the underneath Co/Ni magnetic layers. Indeed, except for the topmost layers of Ta (in case of the Cu/Ta capping layer) and for the Pd layer, all the elements were detected in their metallic state. This result allows ruling out the occurrence of oxidized phases in the free layer affecting the magnetic and magneto-transport behavior of the samples. As the resolution of the XPS depth profiling is of few nanometers, a detailed analysis of the layers sequence is not possible; however, the results clear

indicate the presence of interdiffused interfaces between the capping layer elements and the Co/Ni multilayer, which may affect the overall physical properties.

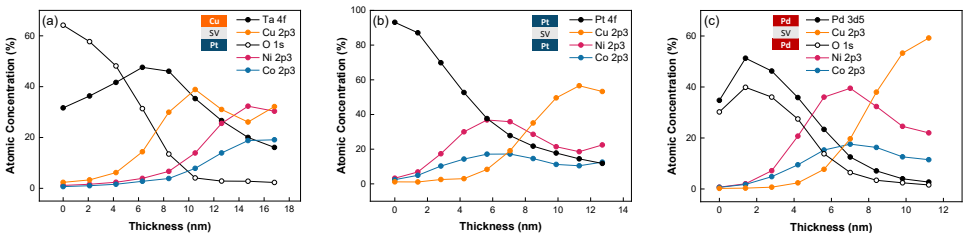


**Figure 6.** Atomic concentration depth profile of the top layers of samples (a) Pt/SV/Cu/Ta, Pd/SV/Pd and Pt/SV/Pt.

To characterize the inner structure of the samples, cross-section TEM and STEM measurements were performed on the same SAF-based GMR-SV thin film stacks analyzed by XPS (i.e., Pt/SV/Cu/Ta, Pd/SV/Pd and Pt/SV/Pt samples). Owing to the difficult in preparing Toenex® samples for (S)TEM analysis, and considering that the magnetic and transport properties of flexible thin films stacks are very similar to those of systems grown on rigid substrates and follow the same trend as a function of the buffer and capping layers, GMR-SVs on SiOx/Si(100) were studied as representative of the investigated samples. **Figures 7a** and **7b** show a typical bright field TEM image of a representative GMR-SV (Pt/SV/Cu/Ta) and the corresponding selected area electron diffraction (SAED) pattern, respectively. The visible diffraction contrast in the bright field image indicates a columnar growth of the magnetic layers, starting from the buffer and going up to the capping layer. This columnar growth is typical of all the analyzed GMR-SVs and SAED measurements reveal, as shown in **Figure 7b**, an oriented growth of the different layers with the {111} atomic planes parallel to the substrate surface. The different layers composing the SV thin film stack are quite well visible in the high-resolution HAADF-STEM images reported in **Figure 7c**. The atoms can be easily identified on all the crystalline layers (see **Figure S3** in the *Supporting Information* for a suitable magnification) indicating the good quality of the entire SV and confirming the {111} oriented growth of the magnetic layers revealed by SAED measurements. The Z-contrast, due to the different atomic number of the elements, is characteristic of this image and allows identifying the Ta buffer and capping layers, as well as the Pt buffer layer and Ru interlayer. However, due to the small differences in the atomic numbers of Co, Ni, and Cu, respectively, it is not possible to resolve these layers in the STEM images. The composition and layer sequence are proved by the EDS line-scan analysis (**Fig. 7d**); the main layers can be distinguished, while the thin alternating layers within the Co/Ni layer cannot be resolved. The analysis also confirms a partial oxidation of the Ta protecting layer in agreement with the XPS analysis.
The same analysis was performed for the samples with Pt and Pd capping layers (**Figure 8**). As for the previous case, the different layers are quite well visible, except for Co, Ni, and Cu that cannot be resolved owing to their similar atomic number. Moreover, the EDS analysis indicate that no oxidation

occurs at the Pt capping layer, while the Pd layer is partially oxidized, as also indicated by the XPS measurements.

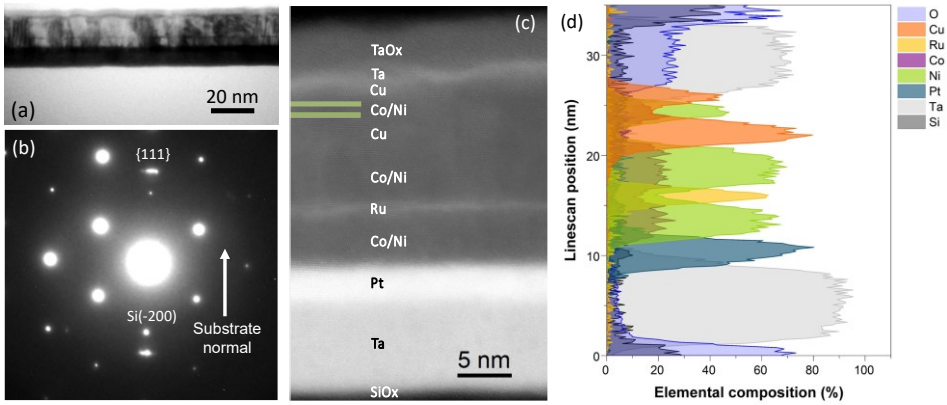


**Figure 7.** Pt/SV/Cu/Ta sample. (a) Bright field TEM image showing the columnar growth of the layers. (b) Corresponding SAED pattern, the arrow indicates the perpendicular to the Si substrate. (c) High-resolution HAADF-STEM image of the whole layers sequence. (d) Quantified EDS line-scan across the layer structure (differences to 100% are due to the carbon signal that is not shown).

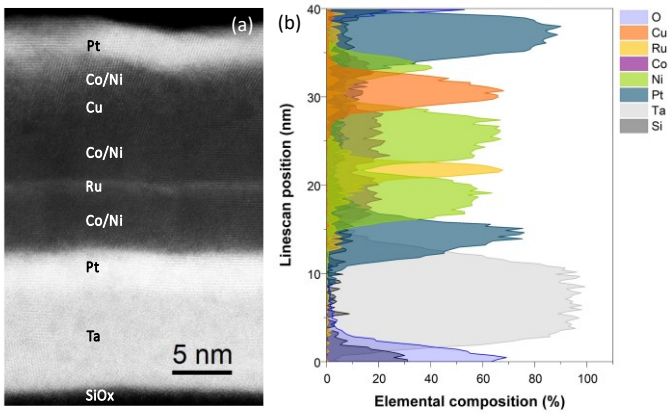

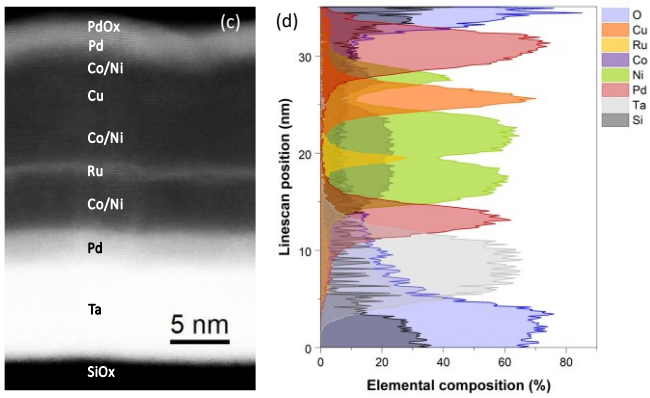


**Figure 8.** (a,b) Pt/SV/Pt and (c,d) Pd/SV/Pd samples. (Left Panels) High-resolution HAADF-STEM images of the whole layers sequence. (Right Panels) Quantified EDS line-scans across the layer structure (differences to 100% are due to the carbon signal that is not shown).

All the investigated samples show a certain level of interdiffusion among the layers. Due to the lower thickness of the free layer ($N_{FL}$ = 2) with respect to that of the Co/Ni layers in the SAF reference electrode ($N_{FL}$ = 6), changes in the intermixing processes are expected to be responsible of the modification of the FL magnetic properties observed for different capping layers. To provide an estimation of the intermixing between the free and capping layers, the first derivative of the elemental line-scan signal was calculated and fitted by a Gaussian function, revealing the full width half maximum (FWHM) values for the Co, Ni, and capping layers for the three investigated samples (see **Figure S4** in the *Supporting Information*). The result of the analysis, reported in **Figure 9** reveals that a much sharper interface is obtained for the system capped with Cu, as evidenced by the lowest FWHM values for Co, Ni, and the $Cu_{capping}$. On the other hand, both Pt and Pd capping layer results in broader interfaces, indicating a higher degree of interdiffusion that seems to be maximum when $Pt_{capping}$ is used.

**Commentato [GV1]:** To be added

According to the differences observed in the magnetic properties of the two classes of systems (SAFs and GMR-SVs) as a function of the capping and buffer layers, a different degree of intermixing is expected to take place also at the interface between the buffer layer and the magnetic stacks. However, the limitations of the TEM line-scan analysis in terms of resolution and sample representativeness, did not allow to highlight significant differences among the samples.

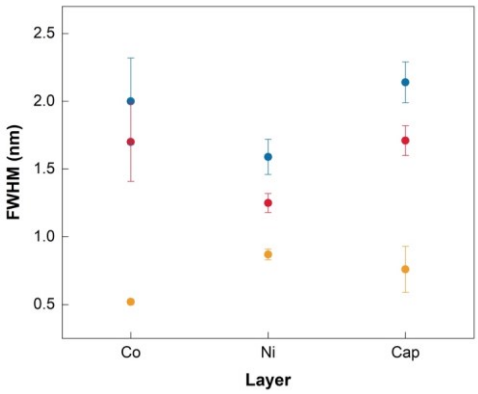


**Figure 9.** Full width half maximum (FWHM) of the first derivative of the elemental line-scan signal for Co, Ni, and capping layers of samples Pt/SV/Cu/Ta (orange dots), Pt/SV/Pt (blue dots) and Pd/SV/Pd (red dots); for the fit parameters refers to Figure S4 in the *Supporting Information*. For each system, the dots indicate, to a first approximation, the diffusion length of Co and Ni towards the capping layer and, vice versa, the diffusion extent of the capping layer (Cap) within the underneath ferromagnetic layer.

## 4. Discussion

The results suggest that the atomic interdiffusion at the interfacial regions may play a major role in determining the physical properties of Co/Ni-based SAF and GRM-SV thin film stacks. The layer intermixing can indeed affect the interface quality and in its turn the PMA of the multilayers[72,73], the interlayer exchange coupling in synthetic antiferromagnetic heterostructures[74,75] as well as the magneto-resistive properties of GMR spin-valve stack[8,76]. In addition, the analysis shows that the magnetic and transport properties strongly depend on the combination of the capping and buffer layers, likely because of a different extension of the interlayer mixing, which depends on the nature of the interfaced atoms as partially evidenced by the STEM analysis for the capping layer. To explain in detail the observed behavior we applied an empirical model recently proposed, which allows predicting the quality of the interface in sputter deposited thin films, by addressing the possible intermixing events that are expected to take place between two different transition metals (the *substrate* and the *growing* materials) during the growth[64]. Depending on the chemical nature, atomic radius, and lattice characteristics, it is possible to obtain different types of interface profiles. Furthermore, for a given set of interfaced atoms, the *effective interface width* ($\sigma$) also depends on the deposition order, i.e., which of the two metals is considered as *substrate* or *growing* element. A successful application of this model was recently demonstrated to disclose the nature of asymmetric interface magnetism in Pt/Co/Pt trilayers and Co/Pt multilayers[63]. To roughly estimate the value of $\sigma$ expected when Pt, Pd and Cu are in contact with the Co layer of the Co/Ni system, we applied the relation[64]

$$\sigma = \frac{1}{0{,}59} A * \left[1 + e^{-B(\gamma_s - \gamma_g)}\right] \qquad (1)$$

where $\gamma_s$ and $\gamma_g$ are the surface energy of the *substrate* and the *growing* metals, respectively (considering γ(Co) = 1.27 eV/atom, γ(Cu) = 0.94 eV/atom, γ(Pd) = 1.23 eV/atom γ(Pt) =1,51 eV/atom), and A and B are two effective parameters accounting for the exchange mechanisms (ballistic and thermodynamically driven) that were experimentally demonstrated to be mainly dependent on the crystal structure of the *substrate* and the *growing* layer (A= 0.27 ± 0.02 nm; B= 1.3 ± 0.5 $eV^{-1}$)[64].
The calculated values of $\sigma$ (nm) for the Co/Pt, Co/Pd, Co/Cu and Pt/Co, Pd/Co, Cu/Co interfaces (i.e., accounting for the different deposition order) are reported in **Figure 10**. According to the model, the interface width decreases by moving from Pt to Pd to Cu when they are capping layers (blue dots); in other words, the Cu interdiffusion towards the Co layer is reduced, with respect to Pt and Pd, when it grows on top of it, in good agreement with the STEM analysis. On the other hand, a different trend is observed when the three metals are considered as buffer layers (purple dots). In this case, when the Cu plays the role of the *substrate* (that means, according to the model, that Co grows on top of a Cu layer) the intermixing events are relevant and the system is characterized by a higher interdiffusion.

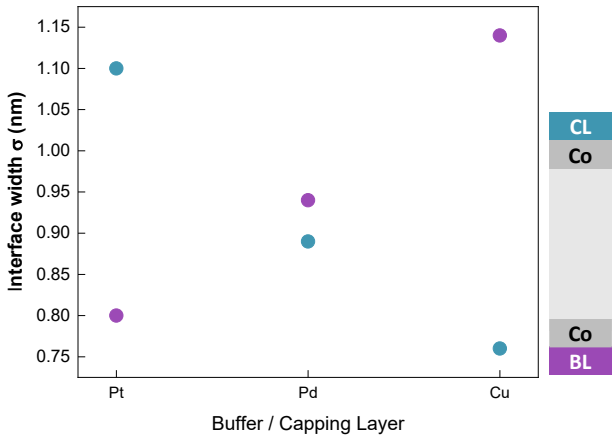


**Figure 10.** Calculated values of the interface width σ for different combinations of Co/Buffer and Capping/Co interfaces.

The magnetic behavior observed in both SAF and SV systems supports the interpretation given by the model. As for the SAF thin film stacks, the higher value of $H_{ex}$ along with a better loop squareness are achieved in the Pt/SAF/Cu sample, i.e., in the system characterized by sharper interfaces, as predicted by the model. However, it is worthwhile noticing that in these samples the contribution on the magnetic properties provided by the buffer layer in terms of structural and morphological order is greater than the effects of the buffer/layer interdiffusion. Indeed, both SAFs grown above the Pt buffer show good properties and the interdiffusion of the Pt capping layer in the Pt/SAF/Pt system slightly affect the magnetic behavior, with a slightly reduced loop squareness and a lower $H_{ex}$ value. In other words, the Pt capping does not damage the structure as much as it does in the Pt/SV/Pt

system, where the FL completely loses its perpendicular anisotropy. Indeed, the high differences provided by the model for the three metals as a function of their buffer/capping role, is fully revealed by the results obtained for the SV system. In this second set of samples, the use of Cu as capping layer allows stabilizing the PMA of the Co/Ni FL, as evidenced by the increase in the loop squareness for both the samples with Pd and Pt buffer layers. The GMR values for these samples benefit from the lower spin polarization induced by the substitution of HM elements with Cu. However, for a fully Cu-substituted spin valve, a worsening of the interface quality induced by the Cu buffer layer imply a modification in the magnetization reversal and a decrease in the GMR values.

Summarizing, for both the systems, the best choice is represented by the Pt-buffer/Cu-capping layers couple, which provide, in agreement with the model, a lower interdiffusion and relatively shaper interfaces. However, the effect of the capping layer on the two systems is different and the reason may be ascribed to the different thickness of the Co/Ni layer interfaced with the capping layer, i.e. $[Co/Ni]_6$ for the SAF and $[Co/Ni]_2$ for the SV. Indeed, at room temperature, the intermixing events are restricted to a limited region of the interface and a reduced effect of such a disorder is expected when the capping layers are interfaced with thicker layers, as in the case of the Pt/SAF/Pt system, where N = 6. In order to further assess this effect, Co/Ni-based GMR-SV with a thicker $[Co/Ni]_{N_{FL}}$ free layer (i.e., $N_{FL}$ = 4) were prepared and capped with a Pt layer, which was found to lead to a strong deterioration of the PMA of the free layer for $N_{FL}$ = 2. As expected, owing to the higher thickness, the Pt diffusion involves, compared to the case $N_{FL}$ = 2, a smaller portion of the free layer (, which therefore shows a squared hysteresis loop (**Figure 11** top panel). As a result, a working PMA GMR spin valve can be obtained by also using a Pt capping layer by increasing the thickness of the free layer (**Figure 11** bottom panel).

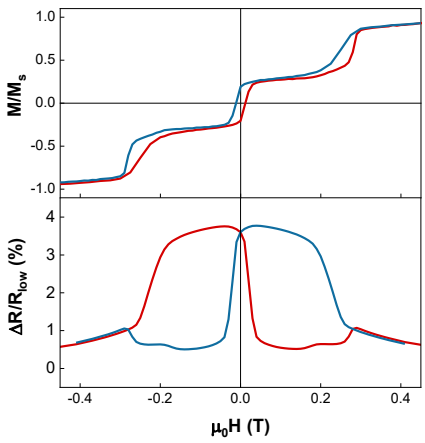


**Figure 11.** Out-of-plane field-dependent magnetization loops (normalized to the saturation magnetization $M_s$, top panel) and corresponding magneto-resistive response ($\Delta R/R_{low}$ *vs.* $H$, bottom panel) of Pt/SV/Pt with a thicker FL (N = 4) deposited on flexible Teonex® tapes.

## 4. Conclusions

In response to the work's objectives, flexible Co/Ni-based PMA SAFs and GMR-SVs with a sizeable GMR ratio (up to 4.4 %) have been prepared with different buffer and capping layers (Pt, Pd, Cu) with the aim of reducing the content of critical elements. All systems, which result robust against mechanical stress, are characterized by microstructural, magnetic and transport properties that slightly differ depending on the combination of the buffer/capping layer. The predictive model developed for sputter deposited metal/metal interfaces has been successfully addressed to discuss the reason at the basis of the different intermixing. The sputtering growth mechanism, which brings to different interfaces depending on the surface energy, the crystal structure of the two materials involved in the growth and their reciprocal growth order, is assumed to play a key role. Sharper interfaces are provided by Pt as bottom layer and Cu as top layer for both SAFs and SVs. In other words, the beneficial effect induced by the Cu capping layer on the magnetic properties may be actually ascribed to the limited interdiffusion processes occurring at the Cu/$[Co/Ni]_N$ interface with respect to the Pd and Pt capping layer. On the other hand, the interdiffusion of both the HM seems to be limited when they are used as buffer layers. Being an interfacial effect, the suitable choice of magnetic layer thicknesses may be considered as an additional tool to reduce the effect of the interdiffusion. The results indicate that complex Co/Ni-based heterostructures with reduced content of PGMs can be deposited on flexible tapes, allowing the development of novel shapeable and sustainable spintronic devices for applications in different fields including wearable electronics, soft robotics, and biomedicine.

## References


(1) Joshi, V. K. Spintronics: A Contemporary Review of Emerging Electronics Devices. *Eng. Sci. Technol. an Int. J.* **2016**, *19*, 1503–1513. https://doi.org/10.1016/j.jestch.2016.05.002.

(2) Dieny, B.; Prejbeanu, I. L.; Garello, K.; Gambardella, P.; Freitas, P.; Lehndorff, R.; Raberg, W.; Ebels, U.; Demokritov, S. O.; Akerman, J.; Deac, A.; Pirro, P.; Adelmann, C.; Anane, A.; Chumak, A. V.; Hirohata, A.; Mangin, S.; Valenzuela, S. O.; Onbaşlı, M. C.; D'Aquino, M.; Prenat, G.; Finocchio, G.; Lopez-Diaz, L.; Chantrell, R.; Chubykalo-Fesenko, O.; Bortolotti, P. Opportunities and Challenges for Spintronics in the Microelectronics Industry. *Nat. Electron.* **2020**, *3*, 446–459. https://doi.org/10.1038/s41928-020-0461-5.

(3) Xiong, D.; Jiang, Y.; Shi, K.; Du, A.; Yao, Y.; Guo, Z.; Zhu, D.; Cao, K.; Peng, S.; Cai, W.; Zhu, D.; Zhao, W. Antiferromagnetic Spintronics: An Overview and Outlook. *Fundam. Res.* **2022**, *2*, 522–534. https://doi.org/10.1016/j.fmre.2022.03.016.

(4) Baltz, V.; Manchon, A.; Tsoi, M.; Moriyama, T.; Ono, T.; Tserkovnyak, Y. Antiferromagnetic Spintronics. *Rev. Mod. Phys.* **2018**, *90*, 15005. https://doi.org/10.1103/RevModPhys.90.015005.

(5) Jungwirth, T.; Marti, X.; Wadley, P.; Wunderlich, J. Antiferromagnetic Spintronics. *Nat. Nanotechnol.* **2016**, *11*, 231–241. https://doi.org/10.1038/nnano.2016.18.

(6) Duine, R. A.; Lee, K.-J.; Parkin, S. S. P.; Stiles, M. D. Synthetic Antiferromagnetic Spintronics. *Natiure Phys.* **2018**, *14*, 217–219.

(7) Makushko, P.; Oliveros Mata, E. S.; Cañón Bermúdez, G. S.; Hassan, M.; Laureti, S.; Rinaldi, C.; Fagiani, F.; Barucca, G.; Schmidt, N.; Zabila, Y.; Kosub, T.; Illing, R.; Volkov, O.; Vladymyrskyi, I.; Fassbender, J.; Albrecht, M.; Varvaro, G.; Makarov, D. Flexible Magnetoreceptor with Tunable Intrinsic Logic for On-Skin Touchless Human-Machine Interfaces. *Adv. Funct. Mater.* **2021**, *31*, 2101089. https://doi.org/10.1002/adfm.202101089.

(8) Hassan, M.; Laureti, S.; Rinaldi, C.; Fagiani, F.; Varotto, S.; Barucca, G.; Schmidt, N. Y.; Varvaro, G.; Albrecht, M. Perpendicularly Magnetized Co/Pd-Based Magneto-Resistive Heterostructures on Flexible Substrates. *Nanoscale Adv.* **2021**, *3*, 3076–3084. https://doi.org/10.1039/d1na00110h.

(9) Legrand, W.; Maccariello, D.; Ajejas, F.; Collin, S.; Vecchiola, A.; Bouzehouane, K.; Reyren, N.; Cros, V.; Fert, A. Room-Temperature Stabilization of Antiferromagnetic Skyrmions in Synthetic Antiferromagnets. *Nat. Mater.* **2020**, *19*, 34–42. https://doi.org/10.1038/s41563-019-0468-3.

(10) Wang, X.; Yang, Q.; Wang, L.; Zhou, Z.; Min, T.; Liu, M.; Sun, N. X. E-Field Control of the RKKY Interaction in FeCoB/Ru/FeCoB/PMN-PT (011 ) Multiferroic Heterostructures. *Adv. Mater.* **2018**, *30*, 1803612. https://doi.org/10.1002/adma.201803612.

(11) Welbourne, E. N.; Vemulkar, T.; Cowburn, R. P. High-Yield Fabrication of Perpendicularly Magnetised Synthetic Antiferromagnetic Nanodiscs. *Nano Res.* **2021**.

(12) Varvaro, G.; Laureti, S.; Peddis, D.; Hassan, M.; Barucca, G.; Mengucci, P.; Gerardino, A.; Giovine, E.; Lik, O.; Nissen, D.; Albrecht, M. Co/Pd-Based Synthetic Antiferromagnetic Thin Films on Au/Resist Underlayers: Towards Biomedical Applications. *Nanoscale* **2019**, *11*, 21891–21899. https://doi.org/10.1039/c9nr06866j.

(13) *New Trends in Nanoparticles Magnetism*, 2021st ed.; Peddis, D., Laureti, S., Fiorani, D., Eds.; Springer Berlin Heidelberg, 2018.

(14) Ma, Z.; Mohapatra, J.; Wei, K.; Liu, J. P.; Sun, S. Magnetic Nanoparticles: Synthesis, Anisotropy, and Applications. *Chem. Rev.* **2021**.

(15) Falciglia, P. P.; Gagliano, E.; Scandura, P.; Bianco, C.; Tosco, T.; Sethi, R.; Varvaro, G.; Agostinelli, E.;

Bongiorno, C.; Russo, A.; Romano, S.; Malandrino, G.; Roccaro, P.; Vagliasindi, F. G. A. Physico-Magnetic Properties and Dynamics of Magnetite (Fe3O4) Nanoparticles (MNPs) under the Effect of Permanent Magnetic Fields in Contaminated Water Treatment Applications. *Sep. Purif. Technol.* **2022**, *296* (May), 121342. https://doi.org/10.1016/j.seppur.2022.121342.

(16) Scialabba, C.; Puleio, R.; Peddis, D.; Varvaro, G.; Calandra, P.; Cassata, G.; Cicero, L.; Licciardi, M.; Giammona, G. Folate Targeted Coated SPIONs as Efficient Tool for MRI. *Nano Res.* **2017**, *10* (9), 3212–3227. https://doi.org/10.1007/s12274-017-1540-4.

(17) Abdolrahimi, M.; Vasilakaki, M.; Slimani, S.; Ntallis, N.; Varvaro, G.; Laureti, S.; Meneghini, C.; Trohidou, K. N.; Fiorani, D.; Peddis, D. Magnetism of Nanoparticles: Effect of the Organic Coating. *Nanomaterials* **2021**, *11* (7). https://doi.org/10.3390/nano11071787.

(18) Parkin, S. S. P. Systematic Variation of the Strength and Oscillation Period of Indirect Magnetic Exchange Coupling through the 3d, 4d, and Sd Transition Metals. *Phys. Rev. Lett.* **1991**, *67*, 3598–3601.

(19) Bruno, P.; Chappert, C. Ruderman-Kittel Theory of Oscillatory Interlayer Coupling. *Phys. Rev. B* **1992**, *46*, 261–270.

(20) Bandiera, S.; Sousa, R. C.; Dahmane, Y.; Ducruet, C.; Portemont, C.; Baltz, V.; Auffret, S.; Prejbeanu, I. L.; Dieny, B. Comparison of Synthetic Antiferromagnets and Hard Ferromagnets as Reference Layer in Magnetic Tunnel Junctions With Perpendicular Magnetic Anisotropy. *IEEE Magn. Lett.* **2010**, *1*, 3000204.

(21) Katine, J. A.; Fullerton, E. E. Device Implications of Spin-Transfer Torques. *J. Magn. Magn. Mater.* **2008**, *320*, 1217–1226. https://doi.org/10.1016/j.jmmm.2007.12.013.

(22) Yang, S.; Ryu, K.; Parkin, S. Domain-Wall Velocities of up to 750 Ms−1 Driven by Exchange-Coupling Torque in Synthetic Antiferromagnets. *Nat. Nanotechnol.* **2015**, *10*, 221–226. https://doi.org/10.1038/NNANO.2014.324.

(23) Back, C.; Cros, V.; Ebert, H.; Fert, A.; Garst, M.; Ma, T. The 2020 Skyrmionics Roadmap. *J. Phys. D. Appl. Phys.* **2020**, *53*, 363001.

(24) Chen, R.; Gao, Y.; Zhang, X.; Zhang, R.; Yin, S.; Chen, X.; Zhou, X.; Zhou, Y.; Xia, J.; Zhou, Y.; Wang, S.; Pan, F.; Zhang, Y.; Song, C. Realization of Isolated and High-Density Skyrmions at Room Temperature in Uncompensated Synthetic Antiferromagnets. *Nano Lett.* **2020**, *20*, 3299–3305. https://doi.org/10.1021/acs.nanolett.0c00116.

(25) Dohi, T.; Duttagupta, S.; Fukami, S.; Ohno, H. Formation and Current-Induced Motion of Synthetic Antiferromagnetic Skyrmion Bubbles. *Nat. Commun.* **2019**, *10*, 5153. https://doi.org/10.1038/s41467-019-13182-6.

(26) Zhou, S.; Zheng, C.; Chen, X.; Liu, Y. Skyrmion-Based Spin-Torque Nano-Oscillator in Synthetic Antiferromagnetic Nanodisks. *J. Appl. Phys.* **2020**, *128*, 033907. https://doi.org/10.1063/5.0013402.

(27) Yu, Z.; Shen, M.; Zeng, Z.; Liang, S.; Liu, Y.; Chen, M.; Zhang, Z.; Lu, Z.; You, L.; Yang, X.; Zhang, Y.; Xiong, R. Voltage-Controlled Skyrmion-Based Nanodevices for Neuromorphic Computing Using a Synthetic Antiferromagnet. *Nanoscale Adv.* **2020**, *2*, 1309–1317. https://doi.org/10.1039/d0na00009d.

(28) Yang, Q.; Wang, L.; Zhou, Z.; Wang, L.; Zhang, Y.; Zhao, S.; Dong, G.; Cheng, Y.; Min, T.; Hu, Z.; Chen, W.; Xia, K.; Liu, M. Ionic Liquid Gating Control of RKKY Interaction in FeCoB/Ru/FeCoB and (Pt/Co)2/Ru/(Co/Pt)2 Multilayers. *Nat. Commun.* **2018**, *9*, 991. https://doi.org/10.1038/s41467-018-03356-z.

(29) Yang, Q.; Zhou, Z.; Wang, L.; Zhang, H.; Cheng, Y.; Hu, Z.; Peng, B.; Liu, M. Ionic Gel Modulation of RKKY Interactions in Synthetic Anti-Ferromagnetic Nanostructures for Low Power Wearable Spintronic Devices. *Adv. Mater.* **2018**, *30*, 1800449 (1-8). https://doi.org/10.1002/adma.201800449.

(30) Bhatti, S.; Sbiaa, R.; Hirohata, A.; Ohno, H.; Fukami, S.; Piramanayagam, S. N. Spintronics Based Random Access Memory : A Review. *Mater. Today* **2017**, *20*, 530–548. https://doi.org/10.1016/j.mattod.2017.07.007.

(31) Ryu, J.; Lee, S.; Lee, K.; Park, B. Current-Induced Spin – Orbit Torques for Spintronic Applications. *Adv. Mater.* **2020**, *32*, 1907148 (1-17). https://doi.org/10.1002/adma.201907148.

(32) Bertacco, R.; Cantoni, M. New Trends in Magnetic Memories. In *Ultra-high density magnetic recording-Storage Materials and Media Designs*; Varvaro, G., Casoli, F., Eds.; Pan Stanford Publishing, 2016.

(33) Yakushiji, K.; Fukushima, A.; Kubota, H.; Konoto, M.; Yuasa, S. Ultralow-Voltage Spin-Transfer Switching in Perpendicularly Magnetized Magnetic Tunnel Junctions with Synthetic Antiferromagnetic Reference Layer. *Appl. Phys. Express* **2013**, *6* (11), 113006 (4pp). https://doi.org/10.7567/APEX.6.113006.

(34) Yakushiji, K.; Kubota, H.; Fukushima, A.; Yuasa, S. Perpendicular Magnetic Tunnel Junctions with Strong Antiferromagnetic Interlayer Exchange Coupling at First Oscillation Peak. *Appl. Phys. Express* **2015**, *8* (8), 083003 (4pp). https://doi.org/10.7567/APEX.8.083003.

(35) Arora, M.; Lee-Hone, N. R.; Mckinnon, T.; Coutts, C.; Hübner, R.; Heinrich, B.; Broun, D. M.; Girt, E. Magnetic Properties of Co / Ni Multilayer Structures for Use in STT-RAM. *J. Phys. D Appl. Phys.* **2017**, *50*, 505003 (11pp).

(36) Arora, M.; Fowley, C.; Mckinnon, T.; Kowalska, E.; Sluka, V.; Deac, A. M.; Heinrich, B.; Girt, E. Spin Torque Switching in Nanopillars With Antiferromagnetic Reference Layer. *IEEE Magn. Lett.* **2017**, *8*, 3100605.

(37) Chang, Y.; Garcia-vazquez, V.; Chang, Y.; Wu, T. Perpendicular Magnetic Tunnel Junctions with Synthetic Antiferromagnetic Pinned Layers Based on [ Co/Pd] Multilayers. *J. Appl. Phys.* **2016**, *113*, 17B909. https://doi.org/10.1063/1.4799974.

(38) Devolder, T.; Couet, S.; Swerts, J.; Liu, E.; Lin, T.; Mertens, S.; Furnemont, A.; Kar, G. Annealing Stability of Magnetic Tunnel Junctions Based on Dual MgO Free Layers and [Co/Ni] Based Thin Synthetic Antiferromagnet Fixed System. *J. Appl. Phys.* **2017**, *121*, 113904.

(39) Li, Z.; Zhang, Z.; Zhao, H.; Ma, B.; Jin, Q. Y. High Giant Magnetoresistance and Thermal Annealing Effects in Perpendicular Magnetic [Co/Ni]N-Based Spin Valves. *J. Appl. Phys.* **2015**, *106*, 013907. https://doi.org/10.1063/1.3158068.

(40) Fukushima, A.; Taniguchi, T.; Sugihara, A.; Yakushiji, K.; Kubota, H.; Yuasa, S. Giant Magnetoresistance in Perpendicularly Magnetized Synthetic Antiferromagnetic Coupling with Ir Spacer. *AIP Adv.* **2018**, *8*, 055925. https://doi.org/10.1063/1.5007304.

(41) Muehlenhoff, C.; Krupinski, M.; Zarzycki, A.; Albrecht, M. Magnetoresistive Effects in Co/Pt-Based Perpendicular Synthetic Antiferromagnets. *IEEE Sens. J.* **2022**, *22* (6), 5588–5595. https://doi.org/10.1109/JSEN.2022.3148205.

(42) Lim, S. Ter; Tran, M.; Chenchen, J. W.; Ying, J. F.; Han, G. Effect of Different Seed Layers with Varying Co and Pt Thicknesses on the Magnetic Properties of Co/Pt Multilayers. *J. Appl. Phys.* **2015**, *117*, 17A731. https://doi.org/10.1063/1.4916295.

(43) Engel, B. N.; England, C. D.; Leeuwen, R. A. Van; Wiedmann, M. H.; Falco, C. M. Interface Magnetic Anisotropy in Epitaxial Superlattices. *Phys. Rev. Lett.* **1991**, *67*, 1910–1913.

(44) Johnson, M. T.; Bloemen, P. J. H.; den Broeder, F. J. A.; de Vries, J. J. Magnetic Anisotropy in Metallic Multilayers. *Reports Prog. Phys.* **1996**, *59* (11), 1409–1458. https://doi.org/10.1088/0034-4885/59/11/002.

(45) Varvaro, G.; Imperatori, P.; Laureti, S.; Cannas, C.; Ardu, A.; Plescia, P.; Capobianchi, A. Synthesis of L10 Alloy Nanoparticles. Potential and Versatility of the Pre-Ordered Precursor Reduction Strategy. *J. Alloys Compd.* **2020**, *846*, 156156 (1-10). https://doi.org/10.1016/j.jallcom.2020.156156.

(46) Speliotis, T.; Varvaro, G.; Testa, A. M.; Giannopoulos, G.; Agostinelli, E.; Li, W.; Hadjipanayis, G.; Niarchos, D. Microstructure and Magnetic Properties of (0 01) Textured L1 0 FePt Films on Amorphous Glass Substrate. *Appl. Surf. Sci.* **2015**, *337*, 118–124. https://doi.org/10.1016/j.apsusc.2015.02.073.

(47) Casoli, F.; Nasi, L.; Albertini, F.; Fabbrici, S.; Bocchi, C.; Germini, F.; Luches, P.; Rota, A.; Valeri, S. Morphology Evolution and Magnetic Properties Improvement in FePt Epitaxial Films by in Situ Annealing after Growth. *J. Appl. Phys.* **2008**, *103* (4). https://doi.org/10.1063/1.2885339.

(48) Varvaro, G.; Agostinelli, E.; Laureti, S.; Testa, A. M.; García-Martin, J. M.; Briones, F.; Fiorani, D. Magnetic Anisotropy and Intergrain Interactions in L10 CoPt(111)/Pt(111)/MgO(100) PLD Granular Films with Tilted Easy Axes. *J. Phys. D. Appl. Phys.* **2008**, *41* (13), 134017 (1-5). https://doi.org/10.1088/0022-3727/41/13/134017.

(49) Shima, T.; Takanashi, K.; Takahashi, Y. K.; Hono, K. Preparation and Magnetic Properties of Highly Coercive FePt Films. *Appl. Phys. Lett.* **2002**, *81* (6), 1050–1052. https://doi.org/10.1063/1.1498504.

(50) Albrecht, M.; Hu, G.; Guhr, I. L.; Ulbrich, T. C.; Boneberg, J.; Leiderer, P.; Schatz, G. Magnetic Multilayers on Nanospheres. *Nat. Mater.* **2005**, *4* (3), 203–206. https://doi.org/10.1038/nmat1324.

(51) Ball, D. K.; Günther, S.; Fritzsche, M.; Lenz, K.; Varvaro, G.; Laureti, S.; Makarov, D.; Mücklich, A.; Facsko, S.; Albrecht, M.; Fassbender, J. Out-of-Plane Magnetized Cone-Shaped Magnetic Nanoshells. *J. Phys. D. Appl. Phys.* **2017**, *50* (11). https://doi.org/10.1088/1361-6463/aa5c26.

(52) Vemulkar, T.; Mansell, R.; Fernández-Pacheco, A.; Cowburn, R. P. Toward Flexible Spintronics: Perpendicularly Magnetized Synthetic Antiferromagnetic Thin Films and Nanowires on Polyimide Substrates. *Adv. Funct. Mater.* **2016**, *26* (26), 4704–4711. https://doi.org/10.1002/adfm.201505138.

(53) Melzer, M.; Makarov, D. A Review on Stretchable Magnetic Field Sensorics. *J. Phys. D Appl. Phys. Top.* **2020**, *53*, 083002 (1-34).

(54) Andrieu, S.; Hauet, T.; Gottwald, M.; Rajanikanth, A.; Calmels, L.; Bataille, A. M.; Montaigne, F.; Mangin, S.; Otero, E.; Ohresser, P.; Le Fèvre, P.; Bertran, F.; Resta, A.; Vlad, A.; Coati, A.; Garreau, Y. Co/Ni Multilayers for Spintronics: High Spin Polarization and Tunable Magnetic Anisotropy. *Phys. Rev. Mater.* **2018**, *2* (6), 64410. https://doi.org/10.1103/PhysRevMaterials.2.064410.

(55) Davies, J. E.; Gilbert, D. A.; Mohseni, S. M.; Dumas, R. K.; Akerman, J.; Liu, K. Reversal Mode Instability and Magnetoresistance in Perpendicular (Co/Pd )/Cu/(Co/Ni) Pseudo-Spin-Valves. *Appl. Phys. Lett.* **2013**, *103*, 022409.

(56) Tomczak, Y.; Lin, T.; Swerts, J.; Couet, S.; Mertens, S.; Liu, E.; Kim, W.; Sankaran, K.; Pourtois, G.; Tsvetanova, D.; Souriau, L.; Van Elshocht, S.; Kar, G. S.; Furnemont, A. Influence of the Reference Layer Composition on the Back-End-of-Line Compatibility of Co/Ni-Based Perpendicular Magnetic Tunnel Junction Stacks. *IEEE Trans. Magn.* **2016**, *52* (7), 1–4. https://doi.org/10.1109/TMAG.2016.2515109.

(57) Li, M.; Lau, D.; De Graef, M.; Sokalski, V. Lorentz TEM Investigation of Chiral Spin Textures and Néel Skyrmions in Asymmetric [Pt/(Co/Ni)M/Ir]N Multi-Layer Thin Films. *Phys. Rev. Mater.* **2019**, *3* (6), 64409. https://doi.org/10.1103/PhysRevMaterials.3.064409.

(58) Brock, J. A.; Montoya, S. A.; Im, M.-Y.; Fullerton, E. E. Energy-Efficient Generation of Skyrmion Phases in Co/Ni/Pt-Based Multilayers Using Joule Heating. *Phys. Rev. Mater.* **2020**, *4* (10), 104409. https://doi.org/10.1103/PhysRevMaterials.4.104409.

(59) Gubbiotti, G.; National, I.; Carlotti, G.; Madami, M.; Koyama, T.; Chiba, D.; Casoli, F.; Pini, M. G. Spin Waves in Perpendicularly Magnetized Co Ni (111) Multilayers in the Presence of Magnetic Domains.

*Phys. Rev. B* **2012**, *86* (July), 014401. https://doi.org/10.1103/PhysRevB.86.014401.

(60) Al., M. A. et. Magnetic Properties of Co/Ni Multilayer Structures for Use in STT-RAM. *J. Phys. D. Appl. Phys.* **2017**, *50*.

(61) Palomino, A.; Marty, J.; Auffret, S.; Joumard, I.; Sousa, R. C.; Prejbeanu, I. L.; Ageron, B.; Dieny, B. Evaluating Critical Metals Contained in Spintronic Memory with a Particular Focus on Pt Substitution for Improved Sustainability. *Sustain. Mater. Technol.* **2021**, *28*, e00270. https://doi.org/10.1016/j.susmat.2021.e00270.

(62) MacDonald, W. A.; Looney, M. K.; MacKerron, D.; Eveson, R.; Adam, R.; Hashimoto, K.; Rakos, K. Latest Advances in Substrates for Flexible Electronics. *J. Soc. Inf. Disp.* **2007**, *15* (12), 1075. https://doi.org/10.1889/1.2825093.

(63) Verna, A.; Alippi, P.; Offi, F.; Barucca, G.; Varvaro, G.; Agostinelli, E.; Albrecht, M.; Rutkowski, B.; Ruocco, A.; Paoloni, D.; Valvidares, M.; Laureti, S. Disclosing the Nature of Asymmetric Interface Magnetism in Co/Pt Multilayers. *ACS Appl. Mater. Interfaces* **2022**, *14* (10), 12766–12776. https://doi.org/10.1021/acsami.1c22341.

(64) Chandrasekaran, A.; Kruijs, R. W. E. Van De; Sturm, J. M.; Zameshin, A. A.; Bijkerk, F. Nanoscale Transition Metal Thin Films : Growth Characteristics and Scaling Law for Interlayer Formation. **2019**. https://doi.org/10.1021/acsami.9b14414.

(65) Arora, M.; Hübner, R.; Suess, D.; Heinrich, B.; Girt, E. Origin of Perpendicular Magnetic Anisotropy in Co/Ni Multilayers. *Phys. Rev. B* **2017**, *96* (2), 1–13. https://doi.org/10.1103/PhysRevB.96.024401.

(66) Emori, S.; Beach, G. S. D. Optimization of Out-of-Plane Magnetized Co/Pt Multilayers with Resistive Buffer Layers. *J. Appl. Phys.* **2011**, *110*, 033919. https://doi.org/10.1063/1.3622613.

(67) Pauw, L. J. Van der. A Method of Measuring Specific Resistivity and Hall Effect of Discs of Arbitrary Shape. *Philips Res. Reports* **1958**, *13*, 1–9.

(68) Gopman, D. B.; Dennis, C. L.; Chen, P. J.; Iunin, Y. L.; Finkel, P.; Staruch, M.; Shull, R. D. Strain-Assisted Magnetization Reversal in Co/Ni Multilayers with Perpendicular Magnetic Anisotropy. *Sci. Rep.* **2016**, *6* (June), 1–8. https://doi.org/10.1038/srep27774.

(69) Natarajarathinam, A.; Tadisina, Z. R.; Mewes, T.; Watts, S.; Chen, E.; Gupta, S. Influence of Capping Layers on CoFeB Anisotropy and Damping. In *Journal of Applied Physics*; 2012.

(70) Gabor, M. S.; Tiusan, C.; Petrisor, T.; Petrisor, T. The Influence of the Capping Layer on the Perpendicular Magnetic Anisotropy in Permalloy Thin Films. *IEEE Trans. Magn.* **2014**.

(71) Mangin, S.; Ravelosona, D.; Katine, J. A.; Carey, M. J.; Terris, B. D.; Fullerton, E. E. Current-Induced Magnetization Reversal in Nanopillars with Perpendicular Anisotropy. *Nat. Mater.* **2006**, *5* (3), 210–215. https://doi.org/10.1038/nmat1595.

(72) Lee-Hone, N. R.; Thanhoffer, R.; Neu, V.; Schäfer, R.; Arora, M.; Hübner, R.; Suess, D.; Broun, D. M.; Girt, E. Roughness-Induced Domain Structure in Perpendicular Co/Ni Multilayers. *J. Magn. Magn. Mater.* **2017**, *441*, 283–289. https://doi.org/10.1016/j.jmmm.2017.05.051.

(73) Shan, Z. S.; Woollam, J. A.; Shen, J. X.; Sellmyer, D. J. Anisotropy and Magneto-Optical Properties of Sputtered Co/Ni Multilayer Thin Films. *IEEE Trans. Magn.* **1994**, *30* (6), 4440–4442. https://doi.org/10.1109/20.334113.

(74) Desai, M.; Misra, A.; Doyle, W. D. Effect of Interface Roughness on Exchange Coupling in Synthetic Antiferromagnetic Multilayers. *IEEE Trans. Magn.* **2005**, *41*, 3151–3153.

(75) Lee, J.; An, G.; Yang, S.; Park, H.; Chung, W.; Hong, J.-P. Thermally Robust Perpendicular Co/Pd-Based Synthetic Antiferromagnetic Coupling Enabled by a W Capping or Buffer Layer. *Sci. Rep.* **2016**, *6*

(February), 21324. https://doi.org/10.1038/srep21324.

(76) Tsymbal, E. Y.; Pettifor, D. G. Perspectives of Giant Magnetoresistance. In *Solid State Physics vol 56*; Ehrenreich, H., Spaepen, F., Eds.; New York: Academic, 2001; pp 113–237.